Supporting Information

Rapid charge-transfer cascade through SWCNT composites enabling low-voltage losses for perovskite solar cells

Severin N. Habisreutinger[1]*, Nakita K. Noel[2,3], Bryon W. Larson[1], Obadiah G. Reid[1,4], Jeffrey L. Blackburn[1]

[1] Chemistry and Nanoscience Center, National Renewable Energy Laboratory, 15013 Denver West Parkway, Golden, CO 80401, United States of America

[2] Department of Electrical Engineering, Princeton University, 41 Olden Street, Princeton, New Jersey 08544, United States of America

[3] Princeton Research Institute for the Science and Technology of Materials, Princeton University, 70 Prospect Ave, Princeton NJ, 08544, USA

[4] Renewable and Sustainable Energy Institute, University of Colorado at Boulder, Boulder, CO 80309, United States of America

Experimental Methods

SWNT Functionalization

Powdered SWCNTs produced by the CoMoCAT process, SWeNT CG200, were purchased from Sigma-Aldrich. They have a diameter range of 0.7−1.4 nm and a relative purity of 90% as the percentage of carbon that is present as SWCNTs. rr-P3HT (3.0 mg, regioregular) was dissolved in 5.00 mL of chlorobenzene and sonicated in a bath sonicator for 60 min. SWCNTs (2.5 mg) were added, as purchased, to the dissolved polymer solution and treated with an ultrasonic probe for 10 min. During the sonication the solution was cooled by an ice bath. After sonication treatment, 10 mL of chlorobenzene was added to improve the solubility of the polymer−nanotube hybrids. The mixture was subsequently centrifuged for 8 min at 10 000g to remove nonfunctionalized SWCNTs and other carbonaceous particles. The precipitate was discarded while the supernatant was recovered. In order to remove the excess polymer 20 mL of toluene was added. The mixture was then heated to 140°C for 60 min to induce aggregation of the functionalized SWCNTs. The aggregates were then removed by centrifugation (6 min at 16 600g). The supernatant containing excess polymer was discarded, and the precipitate was recovered. The pellet of polymer-wrapped nanotubes was subsequently dispersed in 6 mL of chloroform. Immediately prior to spin-coating, the chloroform dispersion was sonicated with an ultrasonic probe for 1 min at low intensity (∼10% of amplitude) to break up bundles.

Solar Cell Fabrication

A glass wafer with a layer of fluorine-doped tin oxide (FTO) (TEC7) was first cleaned with 2-propanol. Thereafter, it was treated for 15 min in UV-Ozone. The electron-accepting SnO2 was prepared by dissolving tin(IV) chloride pentahydrate (SnCl4·5H2O) (Sigma-Aldrich) in 2-propanol (0.05 M) and stirred for 30 min. The solution was spin-coated at 3000 rpm for 30 s, with a ramp of 200 rpm/s. The substrates were then dried at 100 °C for 10 min and annealed at 180 °C for 60 min. For the mixed perovskite precursor, 1.0 M formamidinium iodide (Dyesol), 0.2 M methylammonium bromide (Dyesol), 0.2 M lead bromide (Alfa Aesar), and 1.1 M lead iodide (TCI) were dissolved in a solvent mixture of *N,N*-dimethyformamide (DMF) and N,N-dimethyl sulfoxide (DMSO) (4:1 by volume) and stirred for 30 min at room temperature. For the deposition, 20 µL ofthe precursor solution was spin-coated per substrate in a two-step process, spinning for 10 s at 1000 rpm and 35 s at 6000 rpm, and 10 s before the end ofthe second spin-coating step, the spinning substrate was quenched with 120 µL anisole (Sigma-Aldrich). Thereafter, the perovskite films were annealed at 100 °C. For the HTL, 85-200 mg/mL of 2,20,7,70-tetrakis(N,N-di-p-methoxyphenyl-amine)9,9-spirobifluorene (Lumtec) was dissolved in chlorobenzene (Sigma-Aldrich), to which 33 µL/ml of 4-*tert*-butylpyridine (Sigma-Aldrich) was added. The spiro-OMeTAD was deposited by spin-coating at 3000 rpm for 30 s. The SWCNTs were deposited dynamically by drop-by-drop spin-coating (3000 rpm for 90 s) of 50-200 µL of the SWCNT dispersion. The film was blow-dried with an airgun and let sit to dry at RT for 15 min. Finally, silver electrodes were thermally evaporated onto the HTL.

Current−Voltage Measurements

To measure the performance of the solar cells, simulated AM 1.5 sunlight was generated with a class AAB ABET solar simulator calibrated to give simulated AM 1.5, of 100.0 mW cm^{-2} equivalent irradiance, using an NREL- calibrated KG5 filtered silicon reference cell. The current−voltage curves were recorded with a sourcemeter (Keithley 2400, USA). The solar cells were masked with a metal aperture defining the active area (0.0919 cm2) of the solar cells. Additionally, by removing active material between individual cells on the same glass substrate, single-cell contributions were ensured. Measurements were done in a light-tight sample holder to minimize any edge effects and ensure that the reference cell and test cell were located during measurement in the same spot under the solar simulator.

Time-resolved Microwave Conductivity Measurements

For the TRMC measurements, the CPI nanocrystals were deposited onto quartz substrates (2.5 cm^2 area). The samples are pumped with a 5 ns pulse width beam (640 nm) from an OPO pumped by the third harmonic of an Nd:YAG laser, and probed by microwaves at around 9 GHz. The microwave field is absorbed by photogenerated mobile carriers in the NCs, and its relative change in power ΔP can be measured. The change in microwave power relates to the photoconductivity ΔG through $\Delta P/P = -K\Delta G$ where K is an empirically determined calibration factor for the microwave cavity used in this experiment. The photoconductivity is proportional to the number of charges and their mobility. It can be expressed as $\Delta G = e\beta F_A I_0(\phi\sum\mu)$ where e is the elementary charge, $\beta = 2.2$ is the geometric factor for the X-band waveguide used, I_0 is the incident photon flux, F_A the fraction of light absorbed at the excitation wavelength, ϕ is the quantum efficiency of free carrier generation per photon absorbed and $\sum\mu = \mu_e + \mu_h$ the sum of the mobilities of electrons and holes. Bi-exponential fits of the photoconductivity decay transients were weighted to calculate the average carrier lifetime using the equation: $\tau_{avg} = (A_0\tau_0 + A_1\tau_1)/(A_0 + A_1)$. For a charge-carrier yield of $\phi = 1$, the combined charge carrier mobility at t = 0 can be derived from the sum of the pre-exponential factors ($\sum$A) of the fits.

1. Performance statistics

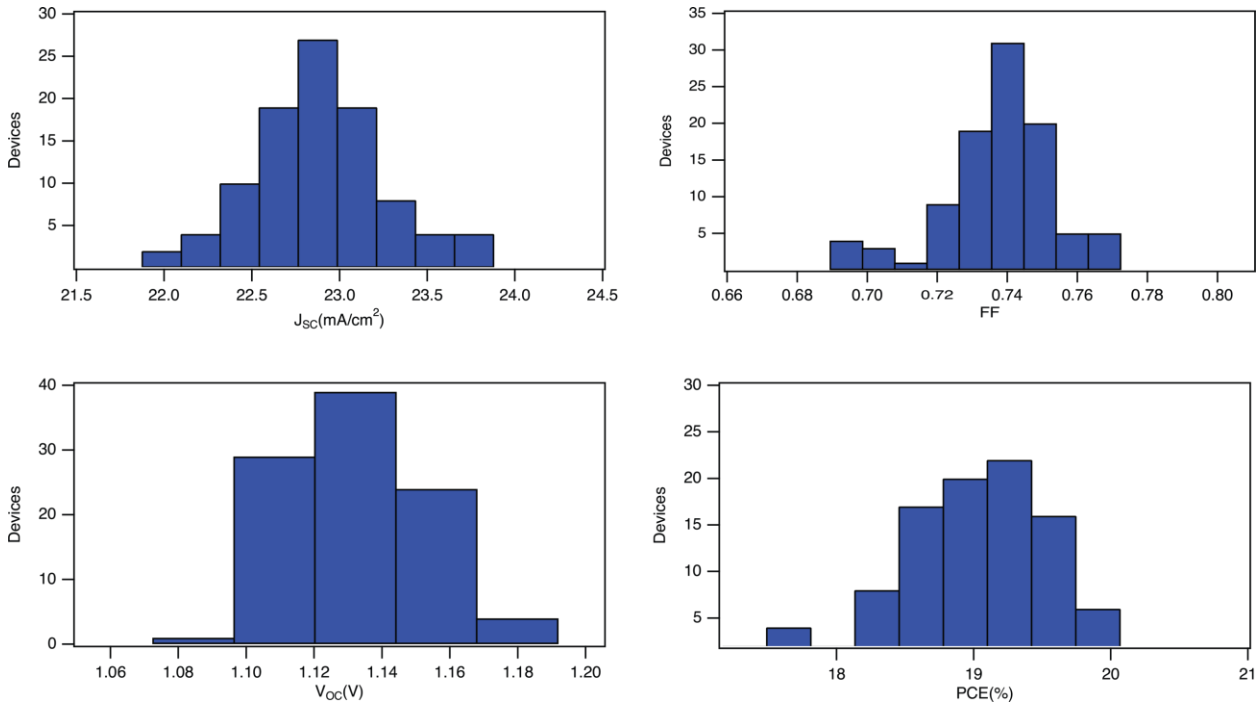

Figure S1 a). Scanned device parameters of devices with spiro-OMeTAD from five different batches

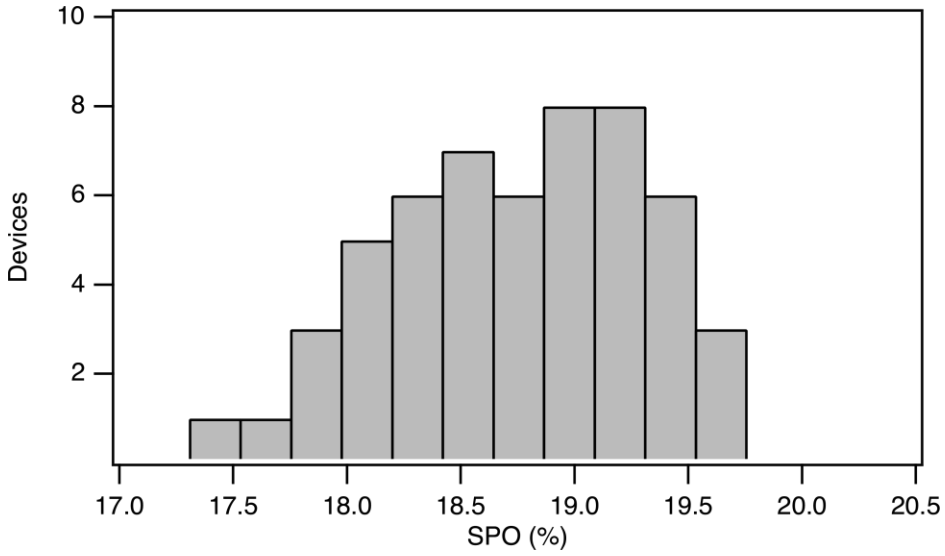

Figure S1 b). Steady-state efficiency of devices with spiro-OMeTAD from five different batches

2. Tauc plot

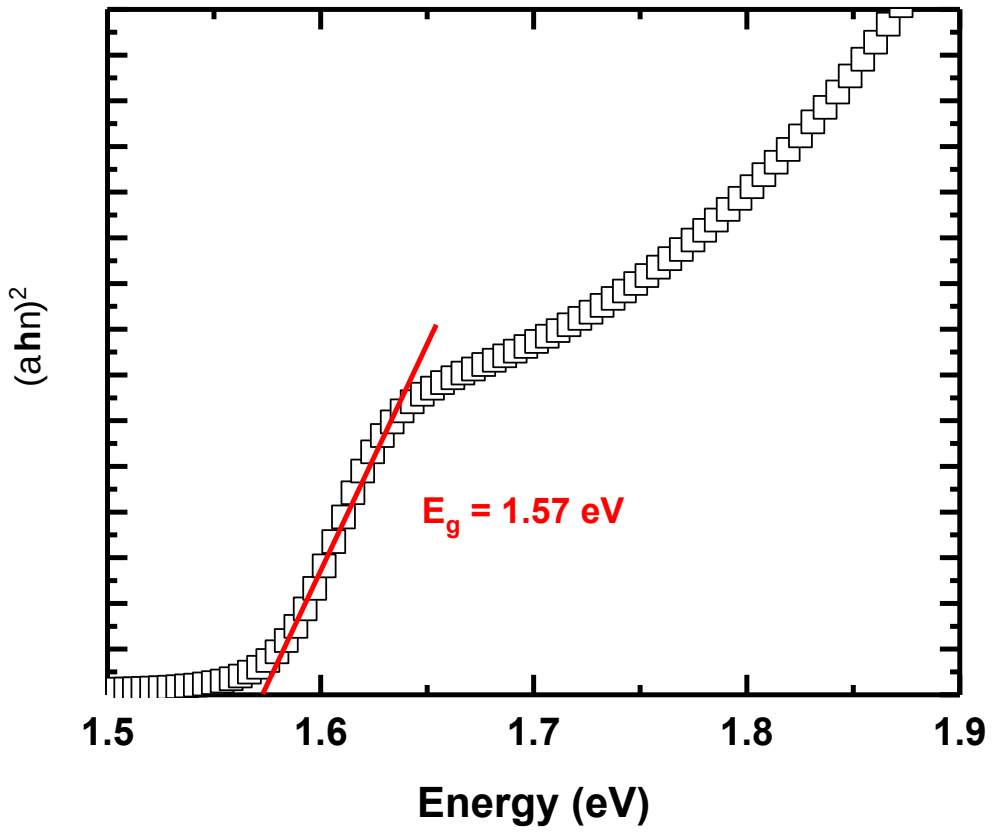

Figure S2: Tauc plot of a perovskite film establishing the bandgap at 1.57 eV

3. P3HT-CG200 Absorption

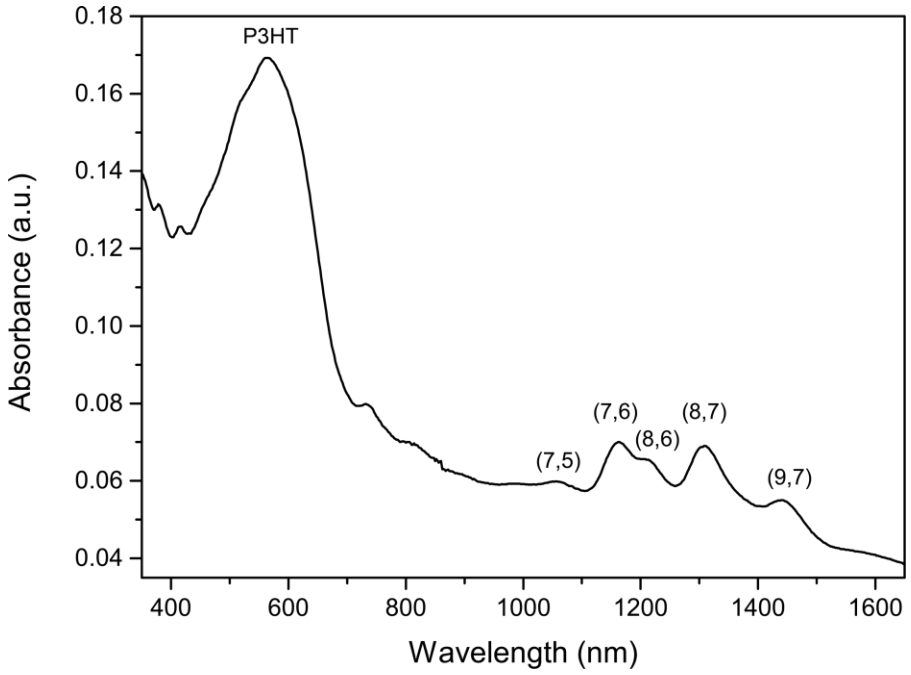

Figure S3: Absorption spectrum of P3HT-wrapped CoMoCAT CG200 SWCNTs. The polymer dissolved in chlorobenzene wraps SWCNTs non-selectively. As a result, no chirality (in brackets) is preferentially functionalized in the final SWCNT distribution and the relative concentrations of chiralities correspond largely to their initial ratios.

4. Undoped spiro-OMeTAD device performance

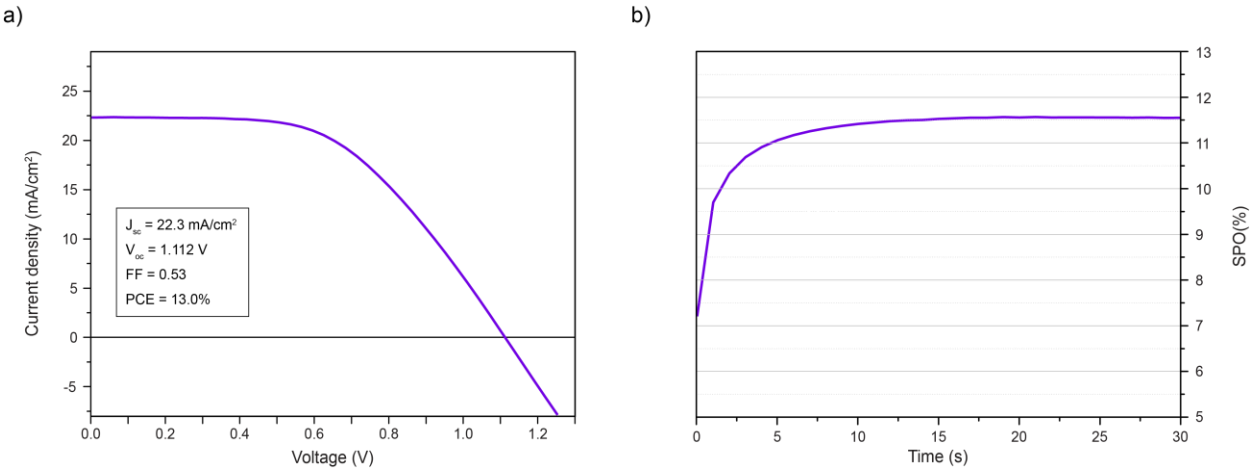

Figure S4: Champion device performance of a device with only undoped spiro-OMeTAD as charge-collection layer. a) current-voltage scan, b) stabilized power output.

5. Dark current for ETL-free samples

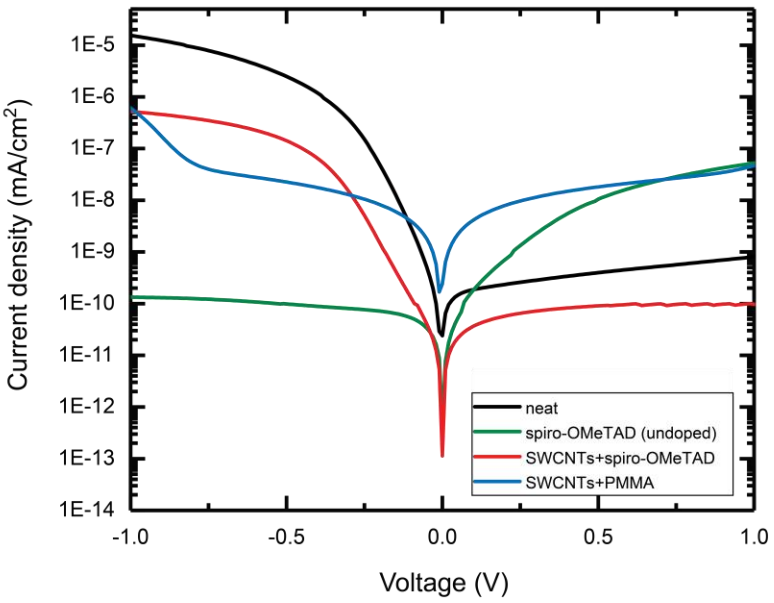

Figure S5: dark current-voltage curves of the various relevant HTL configurations on samples without ETL.

6. TRMC Sensitivity Calculations

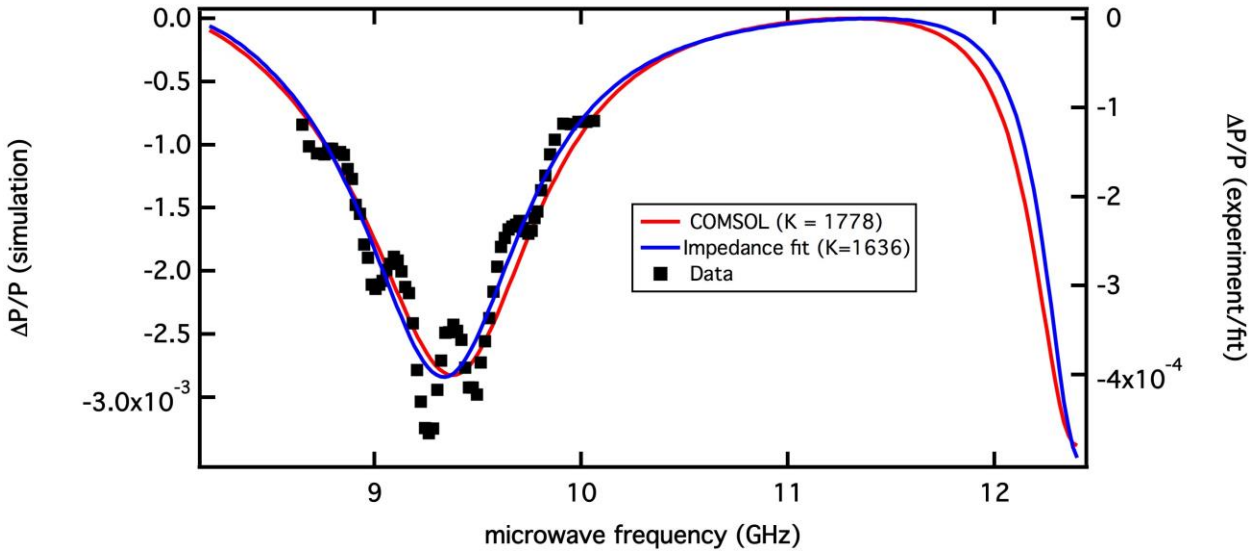

Figure S6: Relative change in microwave power reflection upon photoexcitation of the sample as a function of microwave frequency. Experimental data is shown in black squares, while two different model results are shown by solid lines. The red line comes from a detailed numerical simulation of the microwave waveguide sample holder using COMSOL Multiphysics v4.3a. The blue line gives the result for a simple analytical model using the impedance of each dielectric interface to calculate the overall power reflection coefficient from the sample cell, which is fit to the data. Both calculation methods are detailed in our previous work[4] and yield similar results for the sensitivity factor (K) of the experiment at 9.26 GHz where the present measurements were conducted. We choose to use the value of K calculated using COMSOL, as that model contains more detail and makes fewer approximations than the analytical fit.

7. TRMC of perovskite with PCBM

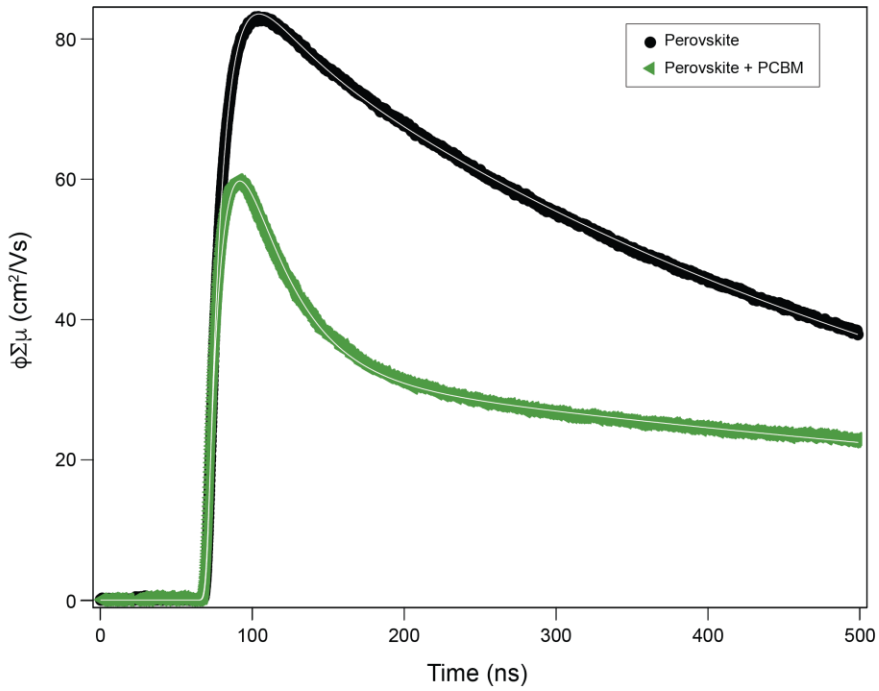

Figure S7: TRMC of bare perovskite and perovskite with a thin layer of PCBM measured with an iris on the cavity to increase the sensitivity of the cavity.

8. Impact of layer thickness of undoped spiro-OMeTAD on the device performance

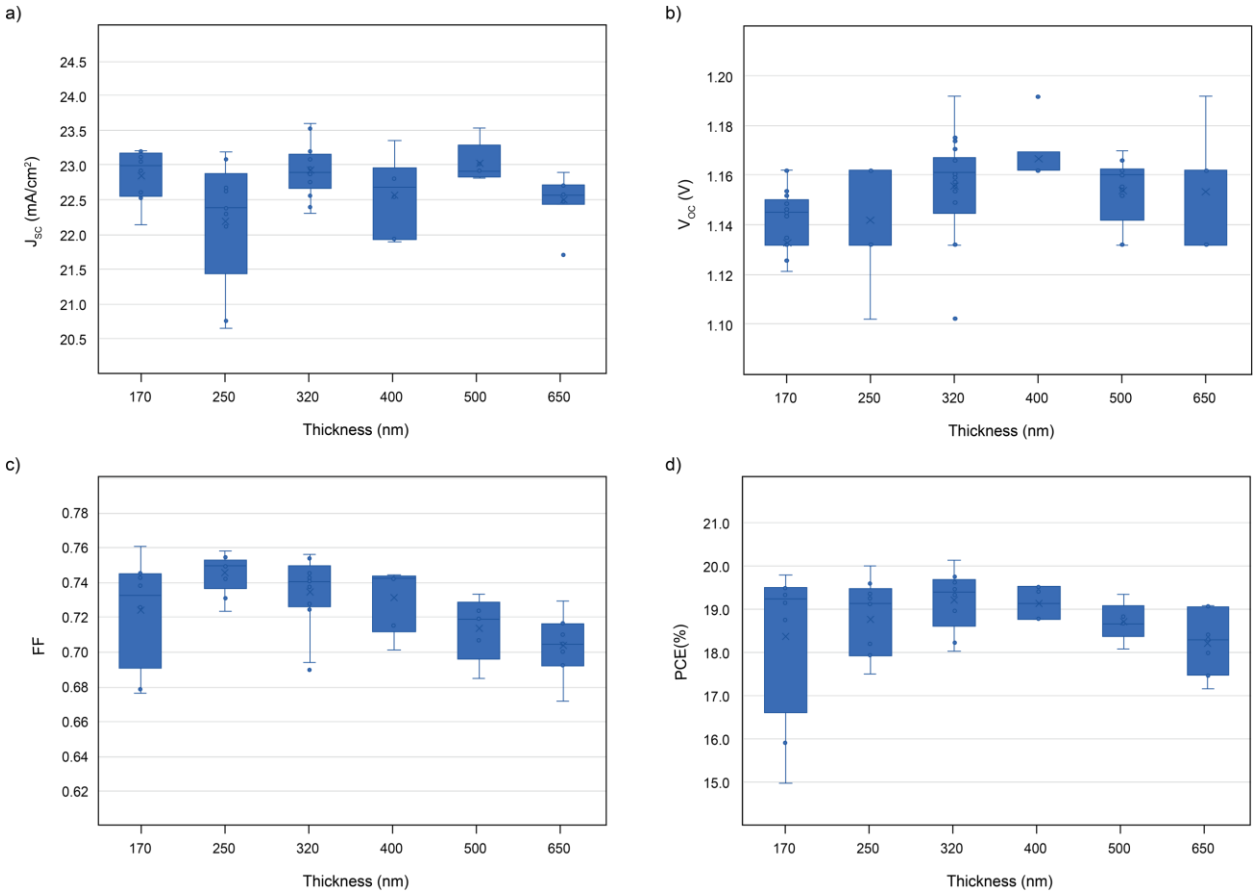

Figure S8: Device performance parameters with an increasing thickness of the undoped spiro-OMeTAD layer, ranging from 170 to 650 nm.

9. Thickness dependence of PMMA

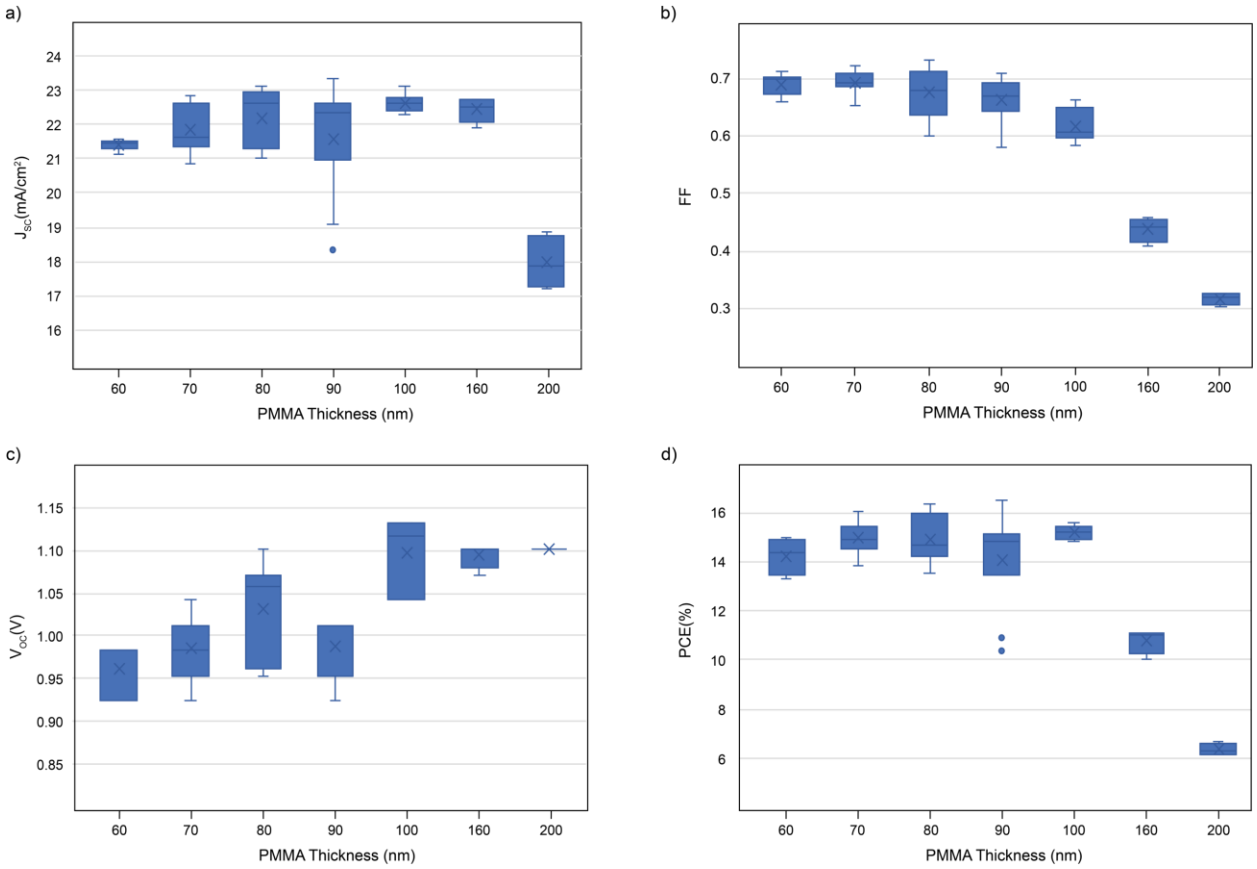

Figure S9: PMMA thickness dependence of the solar cell performance parameters.

10. Device cross section

In the cross sectional scanning electron microscope (SEM) image (Figure S11), SWCNT bundles can be identified at the interface between the perovskite absorber and spiro-OMeTAD. However, imaging the penetration of SWCNTs through the spiro-OMeTAD layer has turned out to be practically impossible, both for cross section as well as top view images. There are conceivably several reasons for why this might be the case. Above all, resolving individual SWCNTs is notoriously difficult in particular in the context of operational devices.
Schuettfort et al. have shown that poly(3-hexylthiophene) (P3HT) wrapping of SWCNTs results in very well individualized SWCNTs preventing the formation of thick bundles.[1] Furthermore, P3HT shows the interesting interaction characteristic when wrapping SWCNTs that it is self-limiting to monolayer coatings on the nanotubes.[2,3] As a result, the nanohybrid structures of P3HT-SWCNTs have diameters on the order of a few nanometers,[1] and therefore beyond the resolution limit for SEM imaging. The multilayer deposition approach (details in the method section), is likely to form a dense lateral layer of SWCNTs, with only few SWCNTs sticking vertically up. We therefore infer the "effective penetration thickness" of the SWCNTs from the double layers using non-conductive PMMA, which can define a layer thickness at which charges can no longer be extracted i.e. too few SWCNTs make direct contact with the electrode because they are fully covered by the second layer.

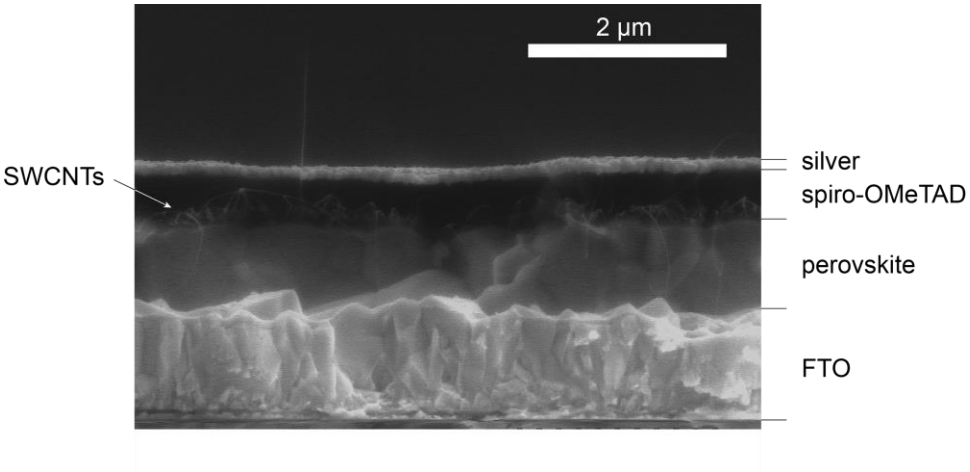

Figure S10: cross sectional SEM image of an operational device stack

11. Thickness regimes of spiro-OMeTAD

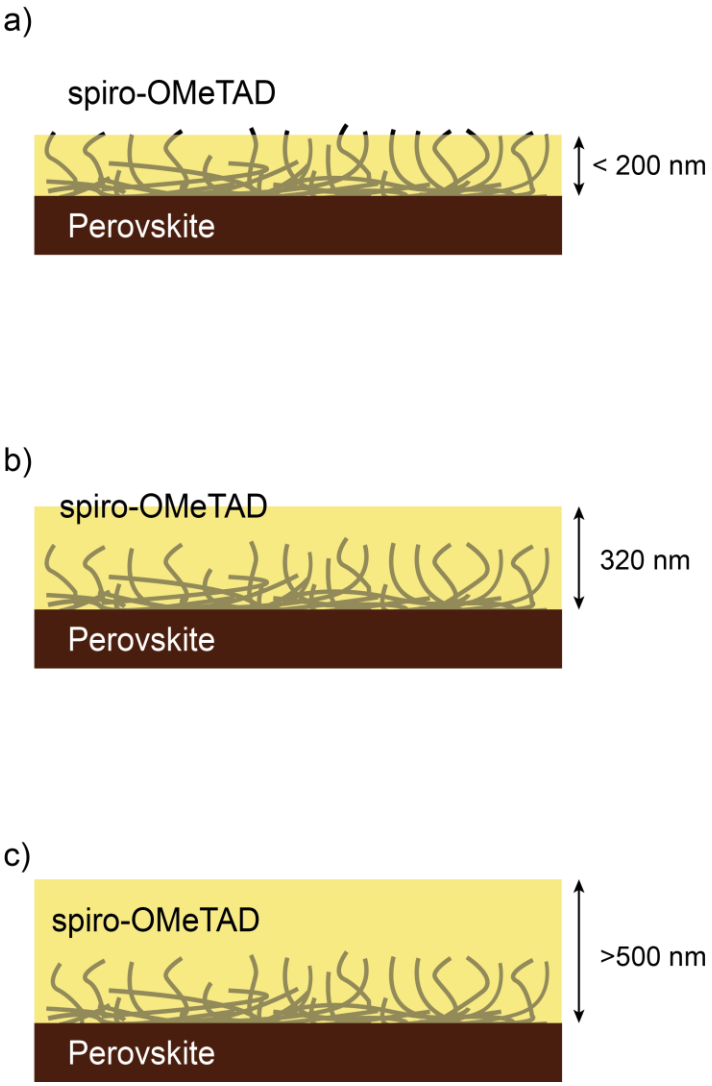

Figure S11: We can identify three thickness regimes for spiro-OMeTAD: a) thin spiro-OMeTAD, where spiro-OMeTAD is thinner than the penetration length of the SWCNTs (< 200 nm); b) optimized spiro-OMeTAD thickness, where spiro-OMeTAD completely covers the SWCNTs but the travel distance for the charges is relatively short; c) thick spiro-OMeTAD, where the capping layer of spiro-OMeTAD is fairly thick and charges have to traverse a relatively large distance through the low-mobility material to reach the electrode.

12. Impact of SWCNT volume on the device performance

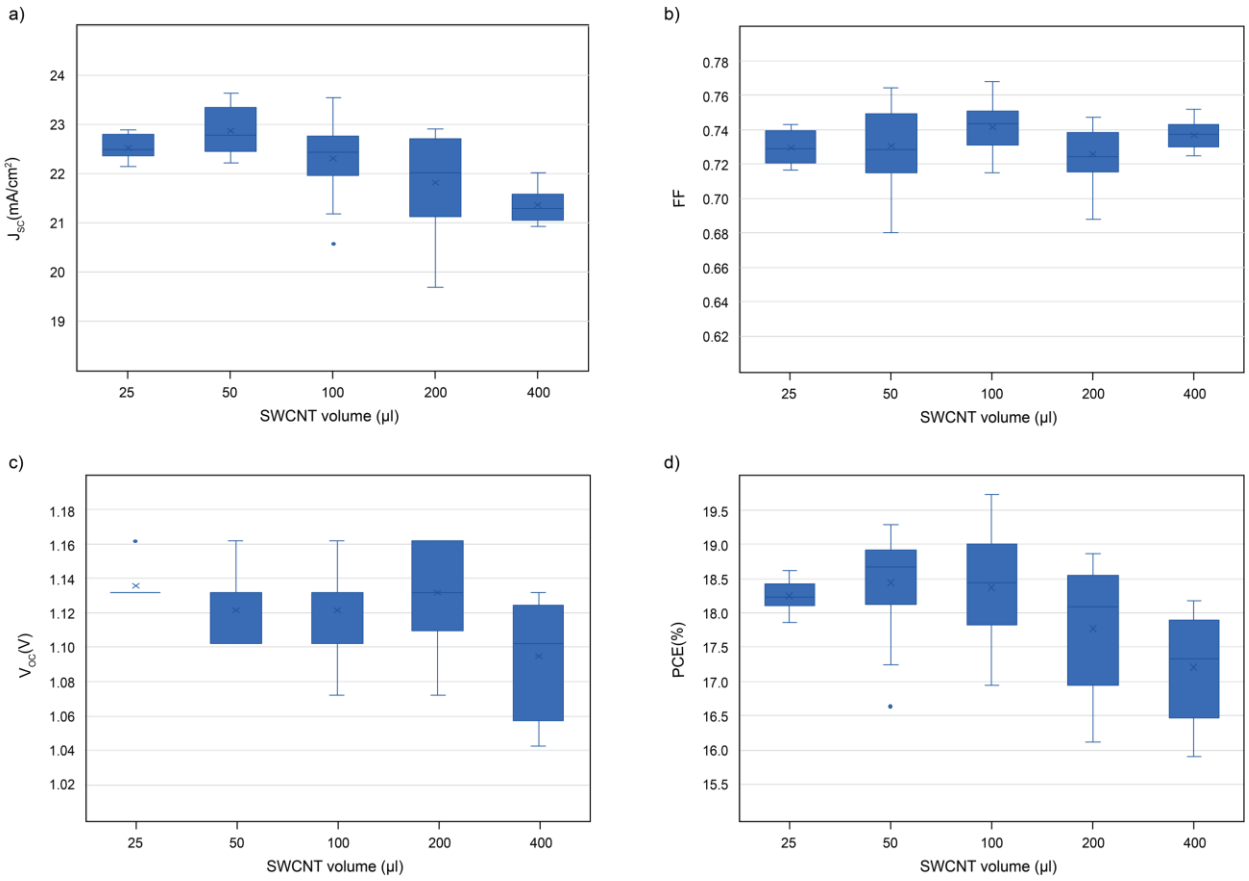

Figure S12: Device performance parameters for different volumes of SWCNTs deposited onto the perovskite

13. Photoluminescence peak of $FA_{0.83}MA_{0.17}Pb(I_{0.83}Br_{0.17})_3$ with 7.5vol% FAH

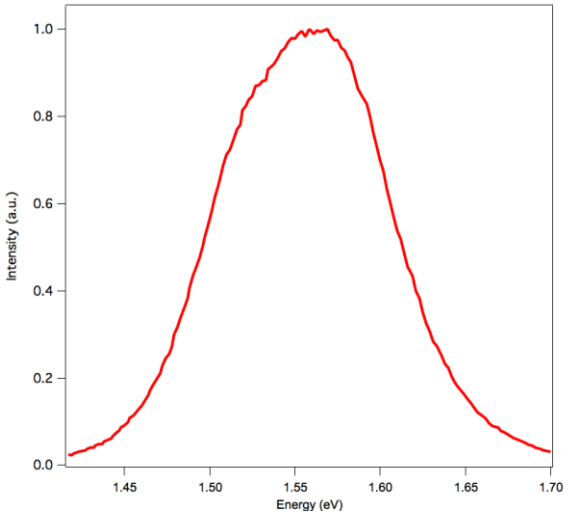

Figure S13: photoluminescence peak of $FA_{0.83}MA_{0.17}Pb(I_{0.83}Br_{0.17})_3$ with 7.5vol% FAH at around 1.57 eV

References

[1] T. Schuettfort, H. J. Snaith, A. Nish, R. J. Nicholas, *Nanotechnology* **2010**, *21*, 25201.

[2] S. D. Stranks, A. M. R. Baker, J. A. Alexander-Webber, B. Dirks, R. J. Nicholas, *Small* **2013**, *9*, 2245.

[3] S. D. Stranks, S. N. Habisreutinger, B. Dirks, R. J. Nicholas, *Adv. Mater.* **2013**, *25*, 4365.

[4] O. G. Reid, D. T. Moore, Z. Li, D. Zhao, Y. Yan, K. Zhu, G. Rumbles, *J. Phys. D. Appl. Phys.* **2017**, *50*, 493002.